Dalton Transactions

ROYAL SOCIETY OF CHEMISTRY

PAPER

View Article Online
View Journal | View Issue

Cite this: *Dalton Trans.*, 2025, **54**, 1038

Bright and persistent green emitting $MgGa_2O_4$:Mn^{2+} for phosphor converted white light emitting diodes†

Reshmi T. Parayil,[a,b] Santosh K. Gupta, *[a,b] Malini Abraham,[c,d] Deepak Tyagi,[e] Subrata Das, [c,d] Mohit Tyagi,[b,f] N. S. Rawat[b,g] and Manoj Mohapatra[a,b]

Narrow band green emitting phosphors have gained widespread attention due to their application in white light emitting diode (wLED) backlight displays. Commercial backlight displays have a broad band green phosphor which limits their performance. In this work, bright, narrow and thermally stable green emitting $MgGa_2O_4$:Mn^{2+} (MGO-Mn) has been synthesized. Time-resolved emission spectroscopy suggested that Mn^{2+} ions are distributed at both Mg^{2+} and Ga^{3+} sites of the MGO spinel, which resulted in a high internal quantum efficiency of 63%. The colour purity of MGO-Mn (76.4%) superseded that of the commercial green phosphor β-SiAlON:Eu^{2+} (59.12%). Doping-induced creation of oxygen vacancies endows MGO-Mn with excellent persistent luminescence with a time duration of more than 900 s upon 4 min charging with 270 nm UV light and persistent radioluminescence of more than 6000 s when charged with X-rays for 1 min. Finally, tunable white LEDs (cool and neutral white LEDs) are fabricated by combining the RGB mixture of the green phosphor with commercial red and blue phosphors along with a 280 nm UV LED chip. This work also showcases the importance of different annealing atmospheres in the photoluminescence and persistent luminescence of the MGO-Mn phosphor.

Received 23rd October 2024,
Accepted 15th November 2024

DOI: 10.1039/d4dt02960g

rsc.li/dalton

1. Introduction

Presently, there is high demand for white light emitting diodes (wLEDs) in backlight display devices, which are the fourth-generation lighting sources having the benefits of low power consumption, long lifetime, high brightness, low heat emission and environmental friendliness.[1,2] The commercial wLED consists of a cerium(III) doped yttrium aluminium garnet phosphor coated on a blue LED chip.[3] Many research studies are going on for the development of a green emitting phosphor with better emission properties. Researchers have reported a good number of green emitting phosphors that find application in areas like white light emitting diodes, backlight displays, optical temperature sensors, anticounterfeiting applications, persistent emission *etc.*[4–10] The most reported green phosphors are rare earth based phosphors which possess many disadvantages such as safety related issues in mining and the high cost of rare earth ions.[11] The reported rare earth based green phosphors include $Li_2Ca_2Si_2O_7$:Eu^{2+},[12] $Ba_2CaZn_2Si_6O_{17}$:Tb^{3+},[13] $Ca_6La_4(SiO_4)_2(PO_4)_4O_2$:$Eu^{2+}$,[14] $NaBaB_9O_{15}$:Eu^{2+},[15] $RbLi(Li_3SiO_4)_2$:Eu^{2+},[16] $CaAl_4O_7$:Ce^{3+},Tb^{3+},[17] $Ca_2YHf_2Al_3O_{12}$:Ce^{3+},Tb^{3+} [18] and $NaSrLa(MoO_4)O_3$:Er^{3+}.[19]

The commercially used green phosphor β-SiAlON:Eu^{2+} emits at 527 nm with an FWHM of 50 nm.[20] Another important green phosphor is $CsPbBr_3$ quantum dots (QDs) with an FWHM value of 20 nm and a high quantum efficiency.[21] Even though QDs have superior emission properties, they cannot withstand the junction temperature of the LEDs and also undergo degradation when exposed to a humid environment.[22] Another important disadvantage is the toxicity associated with Pb, which leads to the search for lanthanide activated green phosphors with narrow band emission. These include $RbNa(Li_3SiO_4)_2$:Eu^{2+} (FWHM ~ 41 nm),[16] $Ba[Li_2(Al_2Si_2)N_6]$:Eu^{2+} (FWHM ~ 57 nm),[23] $SrGa_2S_4$:Eu^{2+} (FWHM ~ 47 nm),[24] and $Ba_2LiSi_7AlN_{12}$:Eu^{2+} (FWHM ~ 61 nm),[25] which have higher green emission efficiency due to the allowed tran-

[a]*Radiochemistry Division, Bhabha Atomic Research Centre, Trombay, Mumbai-400085, India. E-mail: santoshg@barc.gov.in, santufrnd@gmail.com*
[b]*Homi Bhabha National Institute, Anushaktinagar, Mumbai – 400094, India*
[c]*Materials Science and Technology Division, CSIR-National Institute for Interdisciplinary Science and Technology, Thiruvananthapuram, Kerala 695019, India*
[d]*Academy of Scientific and Innovative Research (AcSIR), Ghaziabad-201002, India*
[e]*Chemistry Division, Bhabha Atomic Research Centre, Trombay, Mumbai-400085, India*
[f]*Technical Physics Division, Bhabha Atomic Research Centre, Trombay, Mumbai-400085, India*
[g]*Radiation Physics and Advisory Division, Bhabha Atomic Research Centre, Mumbai-400085, India*

† Electronic supplementary information (ESI) available. See DOI: https://doi.org/10.1039/d4dt02960g

sition of Eu^{2+}(4f–5d). But they have poor thermal stability and high fabrication costs arising from the use of rare earth ions, which paved the urgent need for cheap and thermally stable green emitting phosphors. Transition metal activated (Mn^{2+}) phosphors have been investigated intensely to circumvent the above-mentioned issues. These mainly include $Sr_2MgAl_{22}O_{36}$:Mn^{2+} (FWHM ~ 26 nm),[26] $MgAl_2O_4$:Mn^{2+} (FWHM ~ 35 nm),[6] $BaZnAl_{10}O_{17}$:Mn^{2+} (FWHM ~ 31 nm)[27] and Zn_2SiO_4:Mn^{2+} (FWHM ~ 42 nm).[28]

Another important application of phosphors is in the area of persistent luminescence (PersL) in which the luminescence lasts for a longer duration even after the stoppage of the excitation source which can be UV, visible, IR or high energy X-ray radiation.[29,30] PersL can be used in many areas such as display screens, afterglow toys, bioimaging, information storage, anticounterfeiting *etc*.[31,32] Hu *et al.*[33] reported colour tunable persistent luminescence in oxyfluoride glass which lasted for an hour. Due to the change in the coordination environment of Mn^{2+}, the persistent colour evolves from red to yellow and then to green. Ma *et al.*[34] reported the X-ray excited PersL in MgF_2:Mn^{2+} wherein Ca^{2+} incorporation leads to tunability.

Lanthanide doped phosphors have attracted great attention due to their high color purity and stable narrow band emission, but their high cost and low abundance can limit the scalability of high quality phosphors for different applications. Another important aspect is the tunability in the emission which can be achieved in a transition metal ion doped phosphor and this flexibility is limited in lanthanide-based phosphors. In terms of thermal stability, transition metal ions can maintain the luminescence properties at elevated temperatures compared to lanthanides.

The manganese ion is an ideal luminescent centre that can replace the costly rare-earth ions and can be used as a rare earth free and cost-effective dopant for phosphor applications. Depending upon the crystal field strength of the host matrices, Mn^{2+} can exhibit emission in the green and red regions. In a tetrahedral (weak field) environment, Mn^{2+} exhibits green emission, whereas in an octahedral (strong field) environment, it exhibits red emission. So choosing a host material can control the emission of Mn^{2+} ions.[35,36] Developing a Mn doped material for wLEDs and persistent light emission is a growing field.

In this work we have employed solvent free solid-state synthesis for the preparation of Mn-doped $MgGa_2O_4$ (MGO-Mn) under different annealing atmospheres. The spinel which is annealed under a reducing atmosphere has shown superior emission properties that can be excited by using UV, visible and X-ray radiation with an internal quantum yield of 63%. In addition to that, the material also exhibits longer UV and X-ray

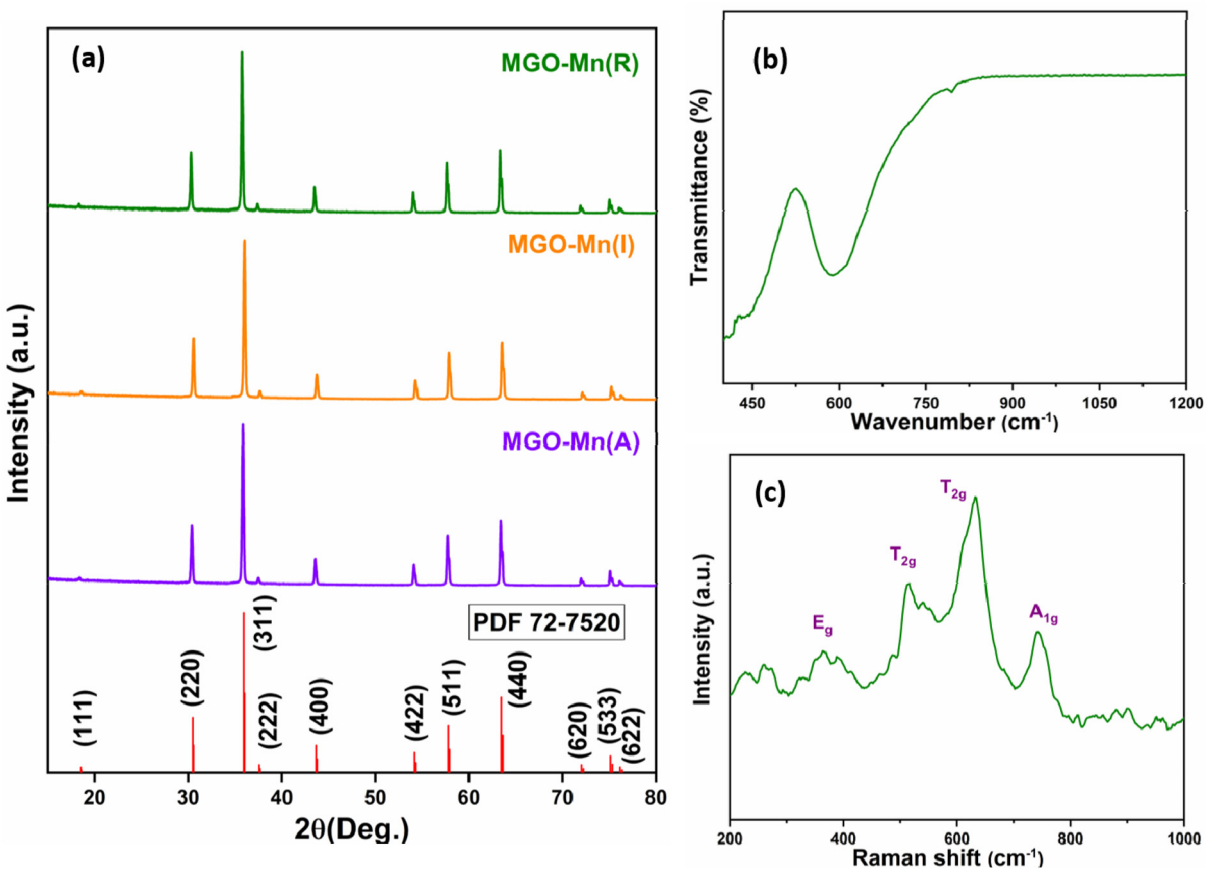

Fig. 1 (a) Powder XRD patterns of MGO-Mn(A), MGO-Mn(I) and MGO-Mn(R), (b) FTIR spectrum and (c) Raman spectrum of MGO-Mn(R)

activated persistent luminescence. Finally, the synthesized green phosphor is mixed with commercial red and blue phosphors in the appropriate composition to produce white light.

2. Experimental

2.1. Synthesis and LED fabrication

The precursors used for the synthesis are MgO (SPEX pure), Ga_2O_3 and $MnCO_3$. The precursors were weighed according to their stoichiometry and ground in a mortar and pestle for 15 min, followed by heating in a muffle furnace at 1350 °C for 5 h under an air atmosphere and then final grinding. This is represented as MGO-Mn(A). Another sample was prepared under an inert atmosphere, which is represented as MGO-Mn(I). The air annealed samples were again annealed under a reducing atmosphere at 1350 °C for 10 h. This sample is represented as MGO-Mn(R). The doping percentage of Mn was 2% in all the above samples.

To assemble a phosphor LED device (pc-LED), the mixture of the as-obtained optimized green phosphor, the BAM:Eu^{2+} blue phosphor, and the Y_2O_3:Eu^{3+} red phosphor (at different ratios) was combined with a 280 nm UV LED chip. Initially, the phosphor mixture was excellently mixed with epoxy resin to obtain phosphor paste. Then the subsequent mixture was coated onto the surface of the 280 nm UV chip to obtain a pc-LED device. Finally, the device features of the obtained pc-LED device were verified using a CCD spectrophotometer, including electroluminescence spectra, chromatic colour coordinates (CIE), colour rendering (CRI), and colour temperature (CCT).

2.2. Instrumentation

X-ray diffraction was performed to confirm the phase purity of the materials on a benchtop Proto X-ray diffractometer with CuKα as the monochromatic source. FTIR measurements were carried out on an Alpha Bruker system in ATR mode.The Raman spectral measurements have been carried out on a micro Raman spectrometer. The FESEM and EDS mapping of the samples

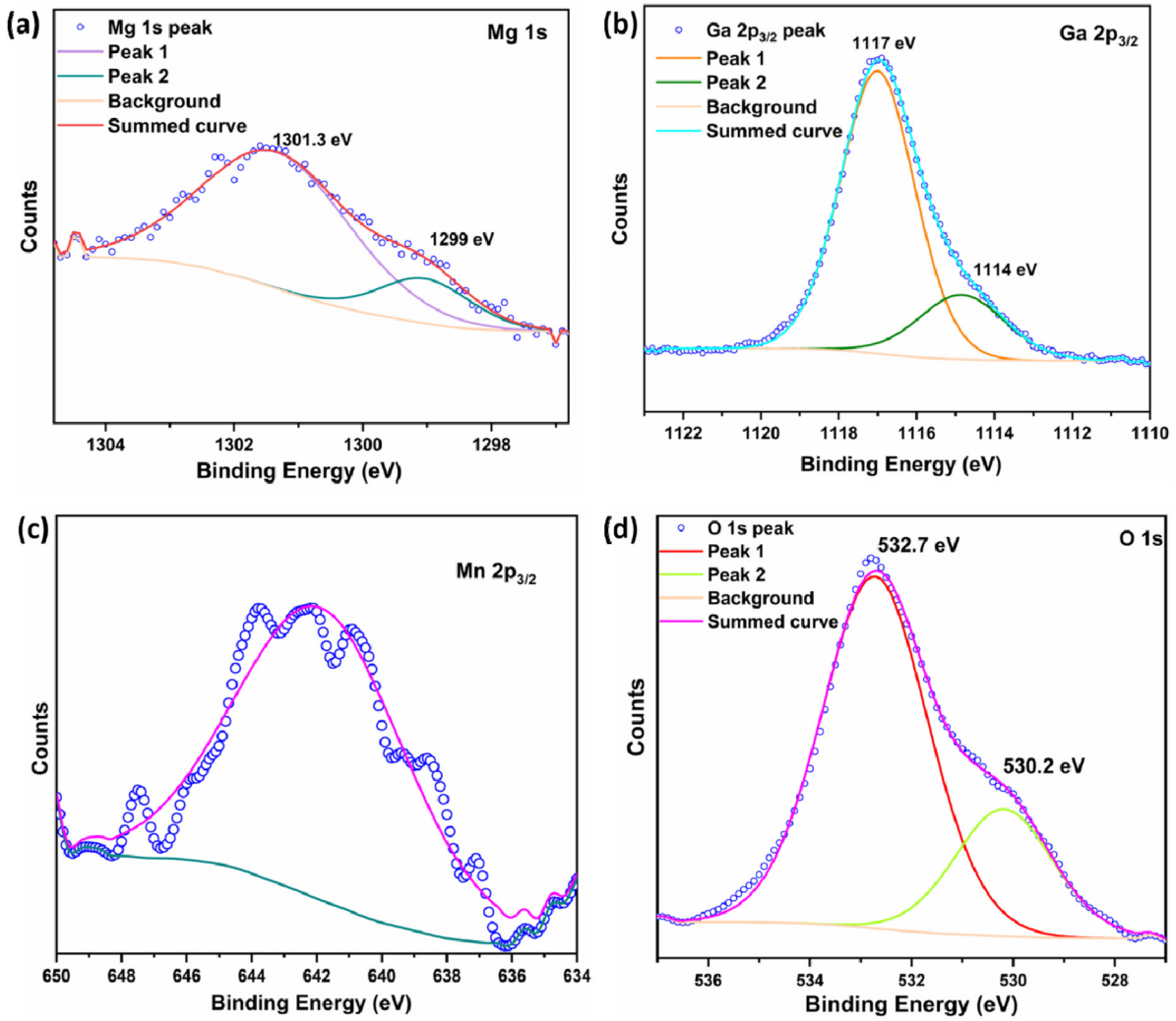

Fig. 2 XPS high resolution spectra of (a) Mg 1s, (b) Ga $2p_{3/2}$, (c) Mn 2p and (d) O 1s of MGO-Mn(R).

were carried out in a Field emission scanning electron microscope (Carl Zeiss Make, GEMINISEM300 Model). All the photoluminescence measurements were done on a fluorescence spectrometer (FLS 1000, Edinburgh make) with a 450 W Xenon lamp as the excitation source. Emission photographs were captured under a 265 nm UV lamp using a Nikon camera. The quantum yield measurements were carried out on an integrating sphere with $BaSO_4$ as the reference. Low-temperature photoluminescence measurements were carried out using a cryostat assembly with the fluorescence spectrometer and liquid nitrogen as the coolant. For decay measurements, a 150 W microsecond flash lamp was used as the excitation source with variable frequencies from 0.1 to 100 Hz. Persistent luminescence measurements were carried out using a PTI QM-400 spectrofluorometer equipped with a 450 W Xenon lamp. Thermoluminescence measurements were performed using a Riso TL/OSL-DA-15 reader system and the signals were recorded at a heating rate of 2 K/s. XPS measurements were carried out on a SPECS instrument with a PHOBIOS 100/150 delay line detector. EPR measurements were performed on a Bruker X-band EPR spectrometer. X-ray excited radioluminescence (RL) measurements were carried out using a customized X-ray generator with a W tube operating at 100 kV and 4 mA. RL emission was recorded with the help of an optical fiber-based Avantes spectrometer. The thermal stability and electroluminescence properties of the obtained samples were determined using a high-sensitivity CCD spectrophotometer (Maya 2000 Pro) by utilizing a 280 nm LED chip. The CIE colour coordinates have been plotted by incorporating the emission values in CIE 1931.

3. Results and discussion

3.1. Phase, vibrational spectroscopy and morphology structural analysis

X-ray powder diffraction has been used to evaluate the phase purity and crystal structure of the synthesized material. The respective XRD patterns are displayed in Fig. 1a. The XRD pattern of the synthesized material matches well with the standard pattern of $MgGa_2O_4$ suggesting that the Mn^{2+} ion is doped into the host lattice with a spinel crystal structure. No other impurity phases are found in the XRD pattern. This observation is consistent with the fact that the ionic radius of the dopant Mn^{2+} is 0.066 nm, which is close to its substitute Mg^{2+}/Ga^{3+} (0.057 nm/0.047 nm) in tetrahedral coordination, whereas that of Mn^{2+} is 0.067 nm, which is close to its substitute Mg^{2+}/Ga^{3+} (0.072 nm/0.055 nm) in octahedral coordination. The space group corresponding to the crystal structure is $Fd\bar{3}m$. In this structure, Mg occupies the tetrahedral site (MgO_4), whereas Ga occupies the octahedral site (GaO_6). Although the crystal structure is spinel, some of the Mg ions can occupy the octahedral site and the same number of Ga can occupy the tetrahedral site, thus forming a partial inverse spinel structure. This creates antisite defects in the crystal structure and the inversion can reach up to 44% depending upon the synthesis methods.[37]

The FTIR spectrum of MGO-Mn(R) is shown in Fig. 1b with two bands at 450 cm^{-1} and 605 cm^{-1}, which correspond to the stretching modes of Ga–O and Mg–O bonds respectively.[38,39] The shoulder peak around 800 cm^{-1} corresponds to the Ga–O vibration in the GaO_4 unit.[40] The FTIR spectra of MGO-Mn(A) and MGO-Mn(I) are shown in Fig. S1†, which have similar bands to those of MGO-Mn(R) except the shoulder peak at 800 cm^{-1}. The shoulder peak corresponds to the inversion of the Ga^{3+} cation, which has also been reported by Naka *et al.*[41] in $CoGa_2O_4$, which confirms that partial inversion is observed in $MgGa_2O_4$.

The Raman spectrum of MGO-Mn(R) is presented in **Fig. 1c.** From group theory analysis, the total number of vibrational modes are $A_{1g} + E_g + 3T_{2g} + T_{1g} + 4T_{1u} + 2A_{2u} + 2E_u + 2T_{2u}$. Among these only five modes, ($A_{1g} + E_g + 3T_{2g}$) are Raman active. The asymmetric peaks are split into doublets which indicate that the spinel has a partially inverted structure. The peak at 741 cm^{-1} corresponds to the A_{1g} mode, the peaks at 633 and 517 cm^{-1} correspond to the T_{2g} mode and the peak at 365 cm^{-1} corresponds to the E_g mode.[34,35]

The FESEM image of the MGO-Mn(R) sample shown in Fig. S2a† depicts irregular shapes with sub-micron size. The high temperature heating has resulted in an appreciable extent of aggregation as well. The EDS mapping of the same is shown in Fig. S2b–S2f†, which confirms the uniform distribution of elements Mg, Ga, O and Mn in the synthesized phosphor.

3.2. X-ray photoelectron spectroscopy (XPS) and electron spin resonance (ESR) spectroscopy

The XPS high resolution spectra of Mg, Ga, Mn and O are shown in Fig. 2. The high-resolution spectra of Mg 1s and Ga $2p_{3/2}$ are shown in Fig. 2a and b, which are asymmetric in nature and the curve can be fitted with two peaks, which confirms that Mg and

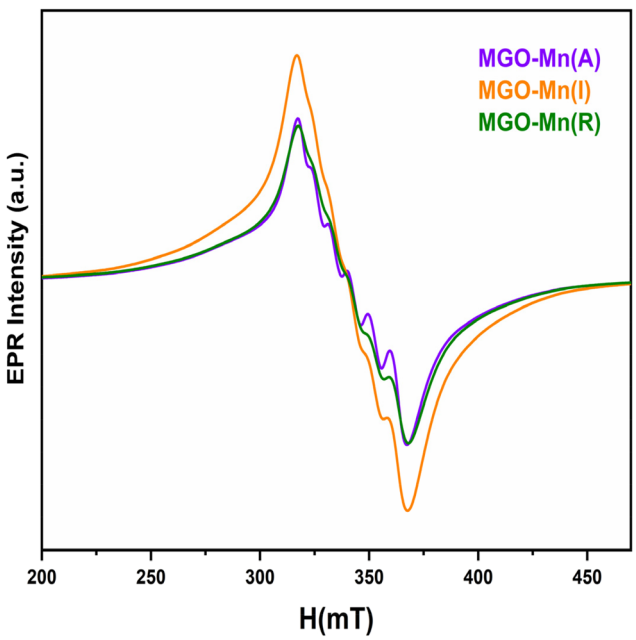

Fig. 3 EPR spectra of MGO-Mn(A), MGO-Mn(I) and MGO-Mn(R).

Ga occupy both octahedral and tetrahedral sites. The peak values of Mg 1s are 1301.3 eV and 1299 eV, which correspond to Mg^{2+} at octahedral and tetrahedral sites respectively.[42] The fitted peak values for Ga $2p_{3/2}$ are 1117 eV and 1114 eV, which correspond to Ga^{3+} at octahedral and tetrahedral sites respectively.[43,44] The high-resolution spectrum of Mn $2p_{3/2}$ is shown in Fig. 2c with a binding energy value of 641.8 eV.[45] The O 1s spectrum is shown in Fig. 2d, which has an asymmetric peak and can be fitted to two peaks with binding energy values of 530.2 and 532.7 eV, which correspond to lattice oxygen and an oxygen vacancy, respectively.[46,47] ^{55}Mn is the major isotope of Mn with 100% natural abundance and nuclear spin $I = 5/2$. Thus, it is expected to give six hyperfine lines due to hyperfine interactions with an electron field. Mn in both +2 and +4 states is EPR active with d^5 and d^3 configurations respectively. Mn^{2+} is expected to show an EPR spectrum close to $g = 2.0$ due to the half-filled configuration, whereas the Mn^{4+} system with the d^3 configuration is expected to show EPR spectra at lower g values than the divalent species. Fig. 3 shows the EPR spectra of the MGO-Mn(A), MGO-Mn(I) and MGO-Mn(R) samples which showed the six hyperfine lines of Mn^{2+}. The MGO-Mn(A) and MGO-Mn(R) phosphors have the same spectral features and the same g values (1.99) as those of MGO-Mn(I). However, the MGO-Mn(I) sample has an unresolved spectrum due to spin exchange broadening and also has higher absorption intensity when compared with MGO-Mn(A) and MGO-Mn(R). This is primarily because of the higher Mn^{2+} concentration which leads to the large spin broadening (50.8 mT).[48]

3.3. Time resolved photoluminescence

Fig. 4a presents the excitation spectrum of MGO-Mn(R) with an emission wavelength of 505 nm. A broad band can be observed in the region from UV to near UV, which comprises host absorption and $Mn^{2+} \rightarrow O^{2-}$ charge transfer. Along with that, three other weak absorption peaks can be seen in the blue region at 380, 425 and 440 nm, which correspond to the forbidden d–d transitions $^4A_1 \rightarrow {}^4T_2$ (^4D), $^4A_1 \rightarrow {}^4T_1$ (^4G) and $^4A_1 \rightarrow {}^4T_2$ (^4G) of Mn^{2+} ions respectively.[49,50] The emission spectra of MGO-Mn(R) with excitation wavelengths of 425 nm

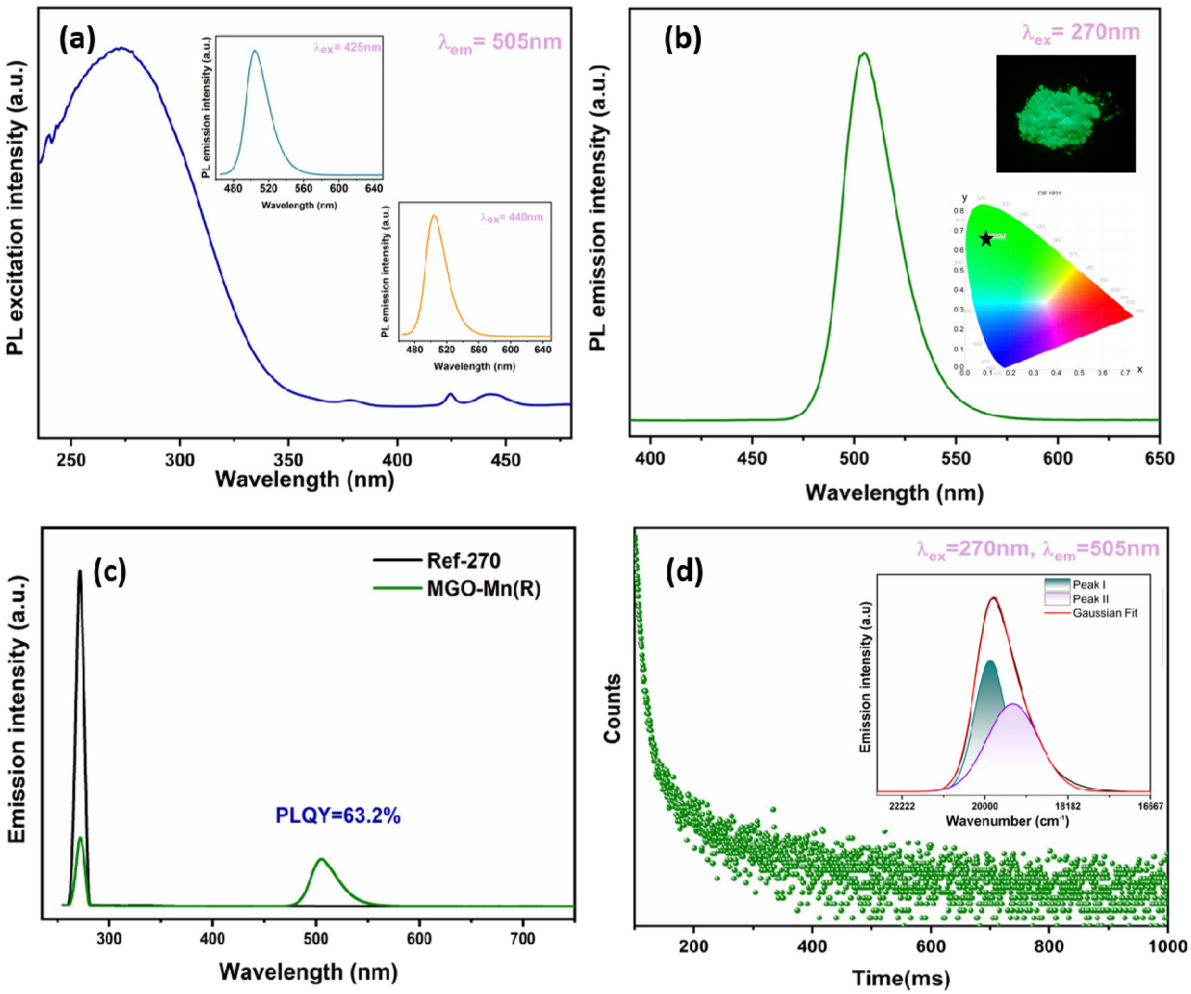

Fig. 4 (a) Excitation spectrum with the inset showing the emission spectra at excitation wavelengths of 425 nm and 440 nm, (b) emission spectrum at an excitation wavelength of 270 nm with the inset showing the corresponding CIE diagram and the digital photograph, (c) spectra for quantum yield and (d) decay plot with the inset showing the peak fitted emission spectrum of MGO-Mn(R).

and 440 nm are shown in the inset of excitation spectrum and the emission spectrum with an excitation wavelength of 270 nm are shown in Fig. 4b; all the emission spectra consist of a broad band in the green region with a peak maximum at 505 nm, which is due to the $^4T_1(^4G) \rightarrow {}^6A_1(^6S)$ d–d transition. The corresponding CIE diagram is shown in the inset with CIE coordinates as (0.085, 0.654). The inset presents the digital image of this sample captured using a Nikon camera under 265 nm UV lamp excitation, which shows bright green colour that can be seen by the naked eye. The FWHM of MGO-Mn(R) is calculated to be 31 nm which is less than that of the commercial green phosphor β-SiAlON:Eu^{2+} (54 nm). This suggests that the MGO-Mn(R) green phosphor can be potentially used in backlight displays. Along with that, the phosphors can be efficiently excited by blue light from 425 or 440 nm. The green emission observed here reveals that Mn^{2+} occupies the low crystal field (tetrahedral coordination).[51] The emission spectra of MGO-Mn(A) and MGO-Mn(I) are shown in Fig. S3.†

To further evaluate the applicability, the internal quantum efficiency (IQE) and external quantum efficiency (EQE) have been calculated by using the integrating sphere method and the spectrum is shown in Fig. 4c. The internal quantum efficiency can be calculated by using the equation:[52]

$$\eta_i = \frac{\int L_S - \int L_R}{\int E_R - \int E_S} \quad (1)$$

The IQE value is obtained as 63.2%. The IQE values for MGO-Mn(A) and MGO-Mn(I) are shown in Fig. S4.†

The external quantum efficiency (EQE) can be calculated by using the equation:

$$\eta_0 = \frac{\int L_S - \int L_R}{\int E_R} \quad (2)$$

The EQE value is obtained as 50%. The green emission at 505 nm is expected to originate from Mn^{2+} occupying the tetrahedral site. In the crystal structure of MGO, as already discussed, both Mg^{2+} and Ga^{3+} have tetrahedral coordination due to the partial inversion, which is confirmed from the FTIR, Raman and XPS studies. In order to determine the site occu-

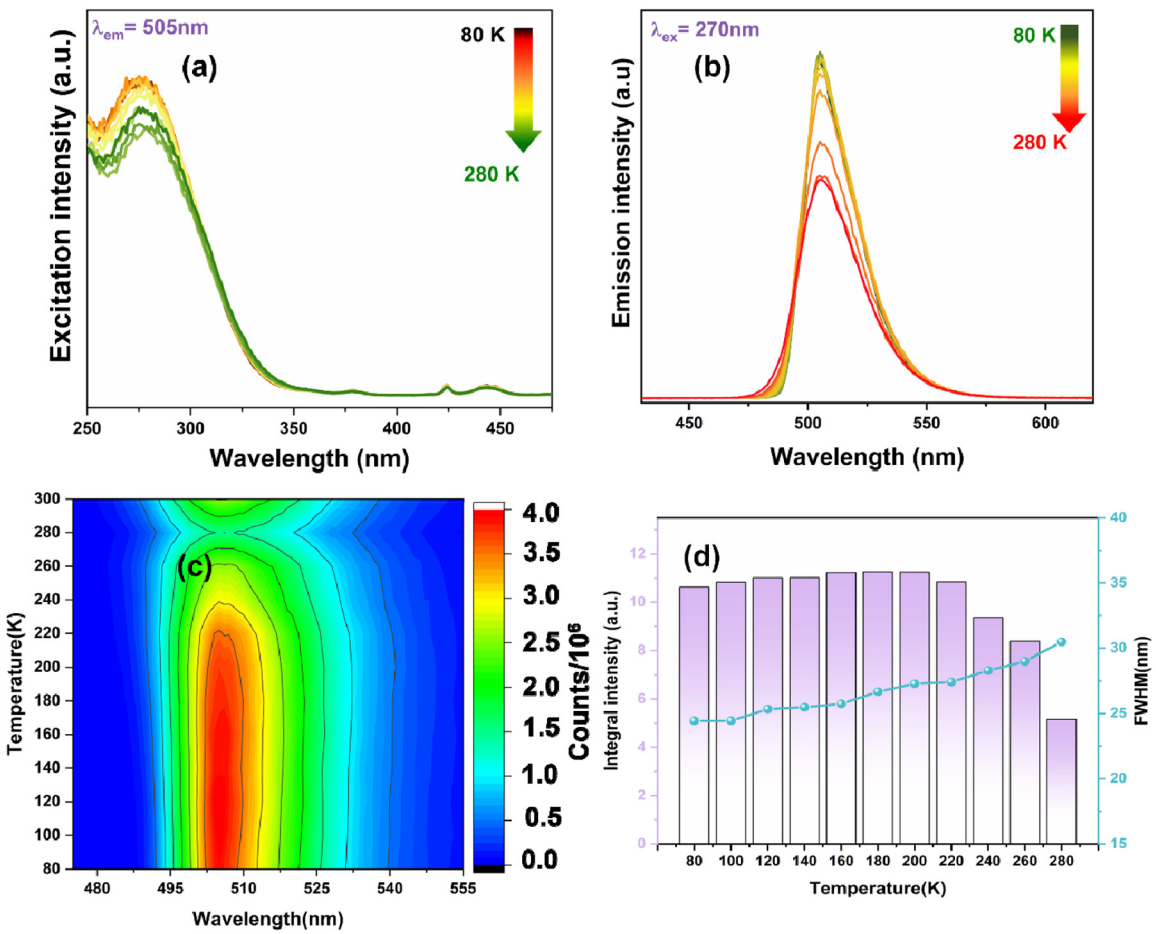

Fig. 5 (a) Excitation spectra in the temperature range of 80 K–280 K with an emission wavelength of 505 nm, (b) emission spectra in the temperature range of 80 K–280 K with an excitation wavelength of 270 nm, (c) contour plot of the emission spectra and (d) plot of the integral intensity and FWHM of MGO-Mn(R) at different temperatures.

Table 1 Comparison of Mn^{2+} and Eu^{2+} activated green phosphors with their emission wavelengths and FWHM values

Green phosphor	Emission wavelength (nm)	FWHM (nm)	Ref.
$Sr_2MgAl_{22}O_{36}:Mn^{2+}$	518	26	26
$MgAl_2O_4:Mn^{2+}$	535	35	6
$SrAl_2Si_2O_8:Mn^{2+}$	517	2	56
$NaGa_8Al_3O_{17}:Mn^{2+}$	510	33	57
$NaGa_{11}O_{17}:Mn^{2+}$	505	29	57
$ZnB_2O_4:Mn^{2+}$	541	41	58
$Zn_2GeO_4:Mn^{2+}$	534	49.5	35
$NaAl_{11}O_{17}:Mn^{2+}$	508	33	59
$Sr_2ZnGe_2O_7:Mn^{2+}$	535	48	60
$LaMgAl_{11}O_{19}:Mn^{2+}$	517	24	61
$Na_2MgAl_{10}O_{17}:Mn^{2+}$	513	27	62
$BaZnAl_{10}O_{17}:Mn^{2+}$	516	31	27
$Rb_3Na(Li_3SiO_4)_4:Eu^{2+}$	527	42	52
$RbLi(Li_3SiO_4)_2:Eu^{2+}$	530	53	16
$Ba_2LiSi_7AlN_{12}:Eu^{2+}$	515	61	25
$(Ba,Sr)SiO_4:Eu^{2+}$	530	72	63
$Ba[Li_2(Al_2Si_2)N_6]:Eu^{2+}$	532	57	23
$MgGa_2O_4:Mn^{2+}(R)$	505	31	This work

pancy of the Mn^{2+} ions, the decay profile was recorded with an excitation of 270 nm and the emission was monitored at 505 nm, which is shown in Fig. 4d. The decay profile follows a bi-exponential decay and can be fitted in the following equation:[1]

$$I(t) = A_0 + A_1 \exp\left(\frac{-t}{\tau_1}\right) + A_2 \exp\left(\frac{-t}{\tau_2}\right) \quad (3)$$

The lifetime values obtained after fitting are 5.6 and 58.3 ms with a relative percentage of 69 and 31, respectively, which confirms that the Mn^{2+} ion occupies two different sites. It can be proposed that the short lifetime value corresponds to Mn^{2+} occupying the Ga^{3+} site whereas the long lifetime corresponds to Mn^{2+} at the Mg^{2+} site. So, the broad emission in the green region can be fitted to two peaks by Gaussian fitting with peak values of 503 and 516 nm.[53,54] We speculate that they correspond to Mn^{2+} occupying the $[MgO_4]$ and $[GaO_4]$ sites, respectively. The substitution of Mn^{2+} at Ga^{3+} can create charge compensating defects such as oxygen vacancy related defects around Mn^{2+}, which is why the peak at 516 nm is broader.

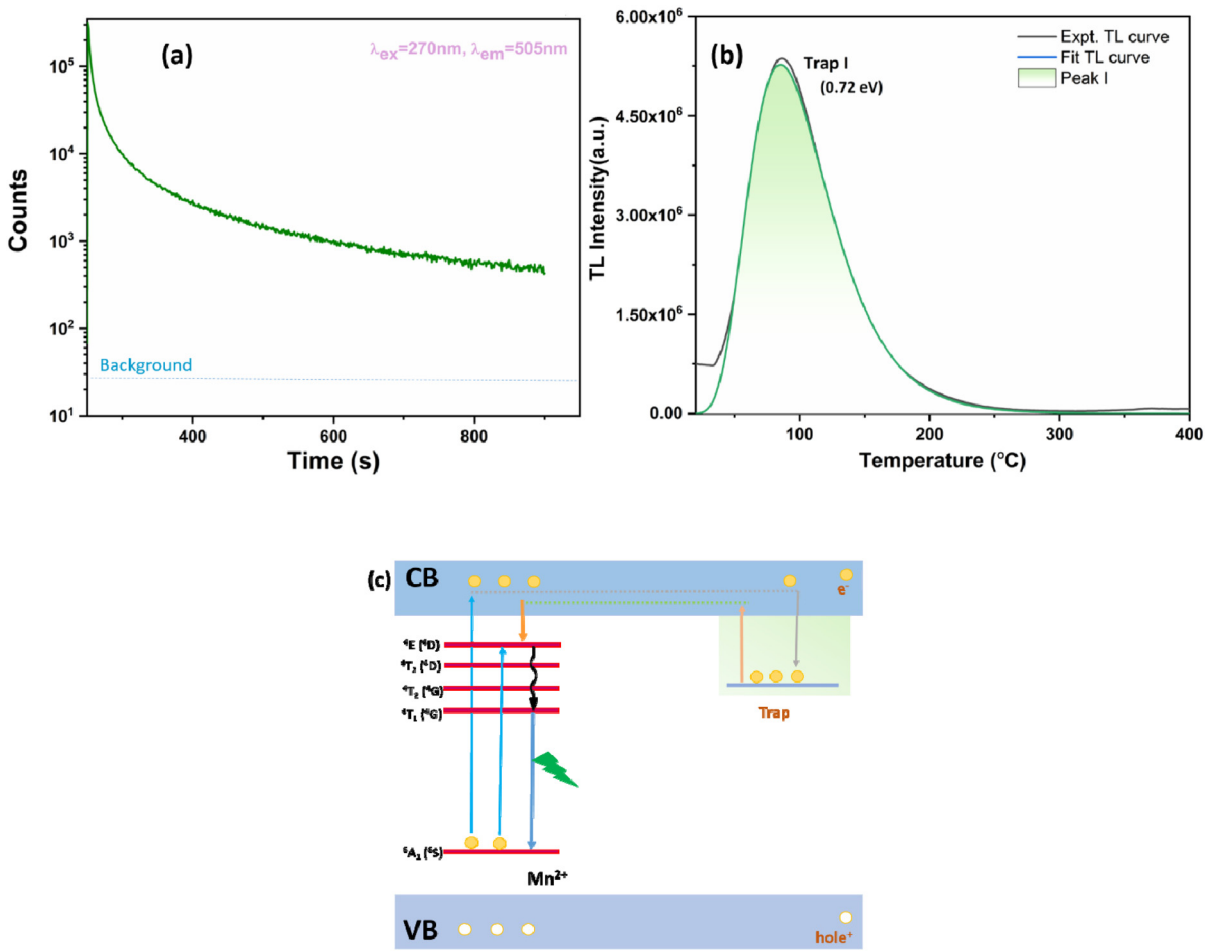

Fig. 6 (a) Persistent decay plot, (b) thermoluminescence spectrum of MGO-Mn(R), and (c) schematics for the persistence mechanism.

The colour purity of the green phosphor can be calculated by using the following equation:

$$\text{Color purity} = \frac{\sqrt{(x_s - x_i)^2 - (y_s - y_i)^2}}{\sqrt{(x_d - x_i)^2 - (y_d - y_i)^2}} \times 100\% \quad (4)$$

Here (x, y) represents the CIE colour coordinates of MGO-Mn (R), (x_i, y_i) represents the CIE colour coordinates of the white light (0.3333, 0.3333) and (x_d, y_d) represents the corresponding colour coordinates of the green monochromatic light source (0.12, 0.82). And the value is calculated to be 76.4%, which is higher than that of the commercial green phosphor β-SiAlON: Eu^{2+} (59.12%), which indicates that the synthesized green phosphor has superior colour purity.

Fig. 5a shows the excitation spectra of MGO-Mn(R) in the temperature range of 80–280 K with an emission wavelength of 505 nm. The same spectral features are observed in the low temperature region with only variation in their intensity. Fig. 5b shows the emission spectra with an excitation wavelength of 270 nm. With an increase in temperature from 80 to 280 K, the emission intensity reduces monotonically, although the emission peak positions barely shift in this temperature range. Fig. 5c shows the corresponding contour plot of the emission profile, and the intensity variation with temperature can be seen from the contour plots. Fig. 5d represents the plot of integral intensity and FWHM as a function of temperature. With an increase in temperature the emission intensity gets reduced whereas the FWHM gets enhanced. When the temperature increases the thermally activated luminous centre more strongly interacts with the thermally activated phonon, which increases the population density of the phonon and thus the electron–phonon interaction becomes more prominent, which results in the enhancement of the FWHM value.[55] Some recently reported Mn^{2+} and Eu^{2+} activated green phosphors with their emission wavelengths and FWHM values are compared in Table 1.

3.4. Persistent luminescence and thermoluminescence

The PersL decay curve is shown in Fig. 6a with an excitation wavelength of 270 nm and an emission wavelength of 505 nm. The decay curve was acquired by illuminating the MGO-Mn(R) sample with 270 nm UV light for 4 min. Afterglow of more

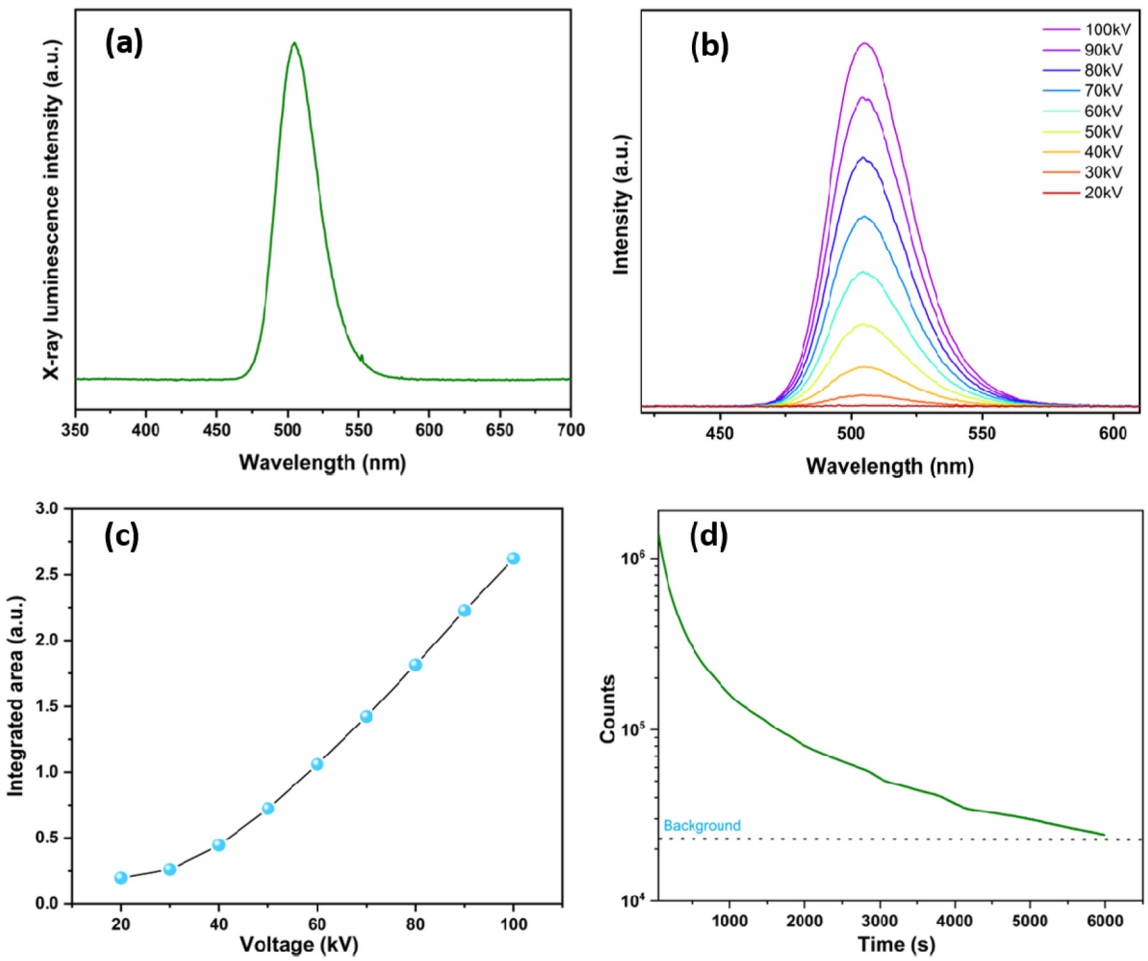

Fig. 7 (a) X-ray excited emission spectrum of MGO-Mn(R), (b) emission spectra of MGO-Mn(R) at different X-ray voltages, (c) plot of the integral area against the X-ray voltage and (d) decay plot of the X-ray excited persistent luminescence of MGO-Mn(R).

than 15 min is observed, which demonstrates that the material is a good persistent luminescent phosphor. In order to correlate the persistence properties, thermoluminescence (TL) was carried out by illuminating the phosphor materials with UV light for 4 min followed by recording the spectrum (Fig. 6b). The trap depth value can be calculated by using the equation:

$$E = T_m/500 \quad (5)$$

Here, E is the activation energy or trap depth and T_m is the maximum temperature in the glow peak. It can be seen that a single shallow trap with a trap depth value of 0.72 eV is observed for MGO-Mn(R). The higher persistent emission in MGO-Mn(R) is due to the higher shallow trap centres compared to MGO-Mn(A) and MGO-Mn(I) which have deep trap centres that quench the persistent emission (Fig. S5†). The XPS measurement has clearly shown the presence of oxygen vacancies in the sample, which played a very crucial role in the persistent luminescence. The oxygen vacancy formation is triggered by aliovalent localization of the majority of Mn^{2+} substitutes at the Ga^{3+} sites, as is already described based on the photophysical measurements. The schematics for the mechanism of persistent luminescence are shown in Fig. 6c. Under UV irradiation, oxygen vacancy related traps can be filled. After stoppage of the excitation the trapped carriers are released from defects *via* the conduction band and to the luminescence center, which is then followed by the recombination of charge carriers giving green persistent luminescence.

The radioluminescence spectrum of MGO-Mn(R) is presented in Fig. 7a, in which the spectral features are the same as those with the UV excitation, which suggests that the origin of emission is from Mn^{2+} ions. Fig. 7b represents the radioluminescence spectra as a function of X-ray voltage starting from 20 kV to 100 kV and a constant current of 4 mA. By increasing the X-ray voltage, the spectral features do not change but the RL intensity increases monotonically, as shown in Fig. 7c.

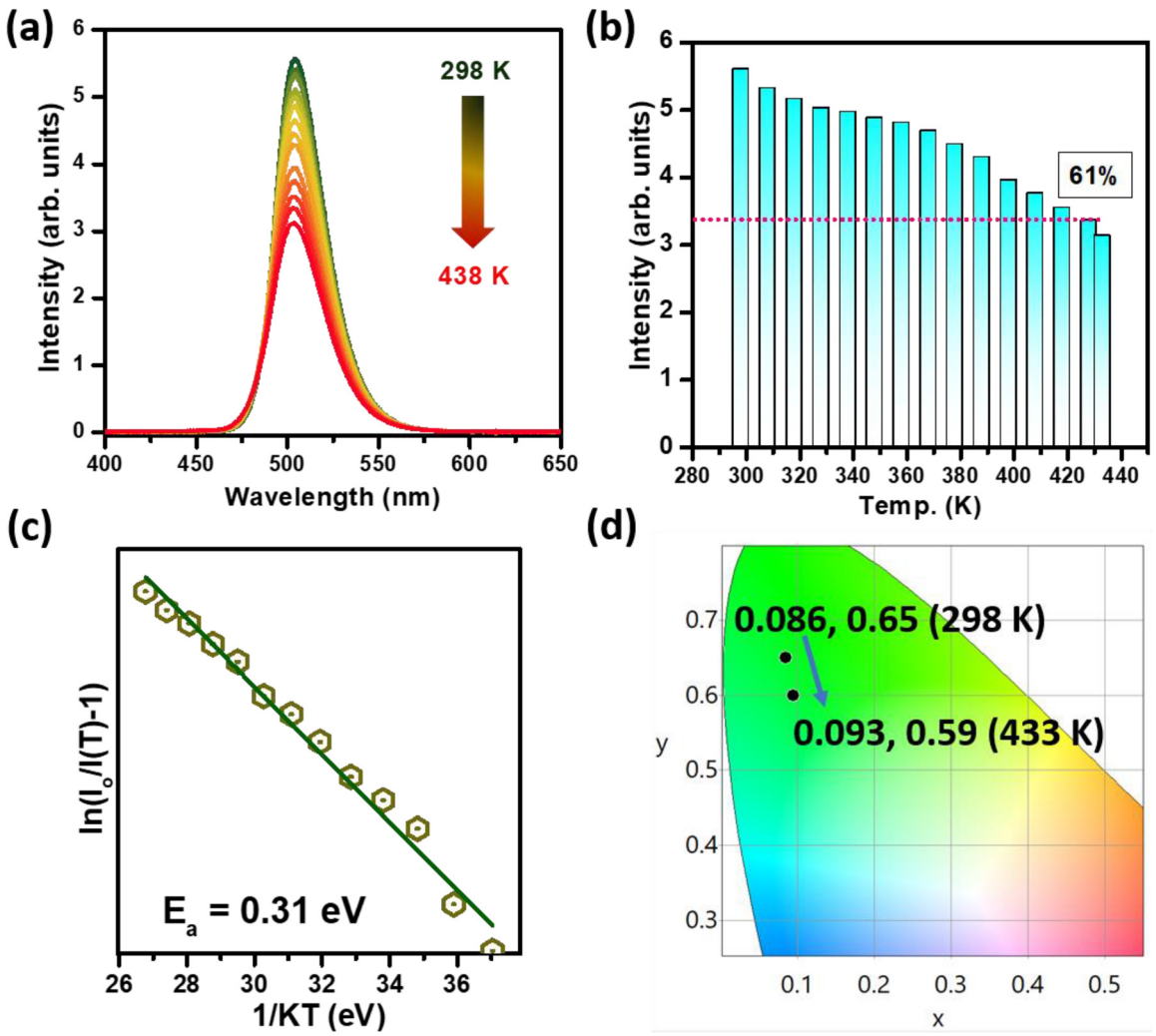

Fig. 8 (a) PL spectra of the MGO-Mn(R) phosphor measured at temperatures from 298 to 438 K under the excitation of a 280 nm UV LED. (b) The Arrhenius fitting of the emission intensity of the MGO-Mn(R) phosphor and the calculated activation energy (E_a) for thermal quenching. (c) Relative intensity of the MGO-Mn(R) phosphor at different temperatures. (d) The CIE variations in the MGO-Mn(R) phosphor at different temperatures.

Another important feature observed is the X-ray excited persistent luminescence of the material which lasts for around 100 min, as presented in Fig. 7d.

3.5. Temperature-dependent photoluminescence

Thermal stability is recognized as a crucial parameter for any phosphor material to be used in devices. Fig. 8a summarizes the emission spectra of the MGO-Mn(R) green phosphor recorded at various temperatures ranging from 298 to 438 K. It is realized that the integrated emission intensity of the measured system reduced gradually with mounting temperatures. However, even at around 423 K, the MGO-Mn(R) green phosphor preserves nearly 61% of its room temperature emission intensity (Fig. 8b). With the help of the Arrhenius plot

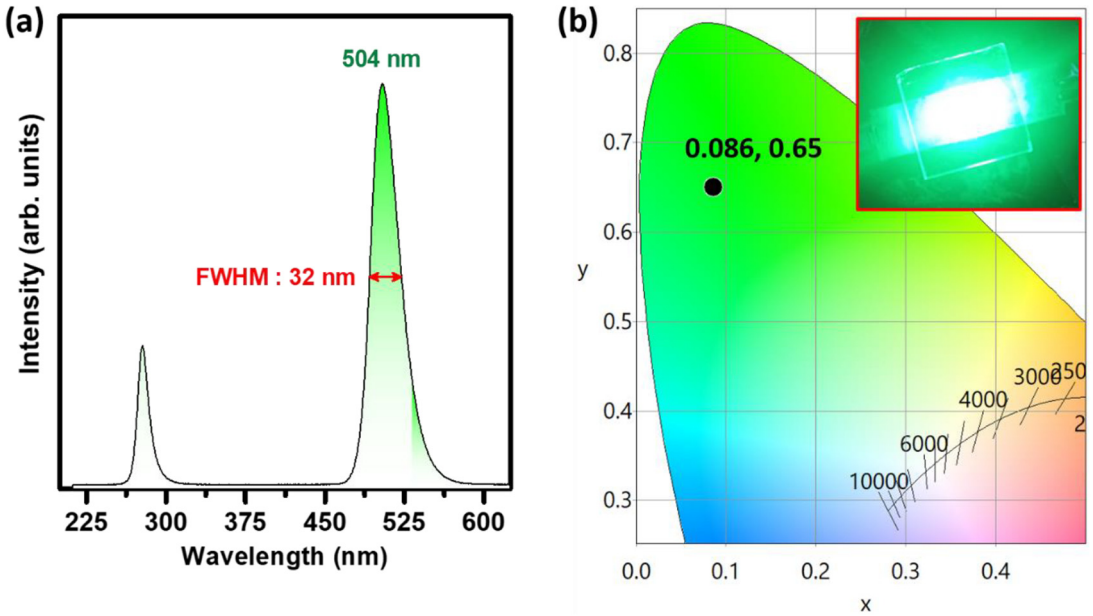

Fig. 9 (a) The EL spectrum of the MGO-Mn(R) phosphor combined with a 280 nm UV LED of current 3 mA. (b) The CIE diagram of the corresponding EL spectrum along with the direct image of the illuminated device (inset).

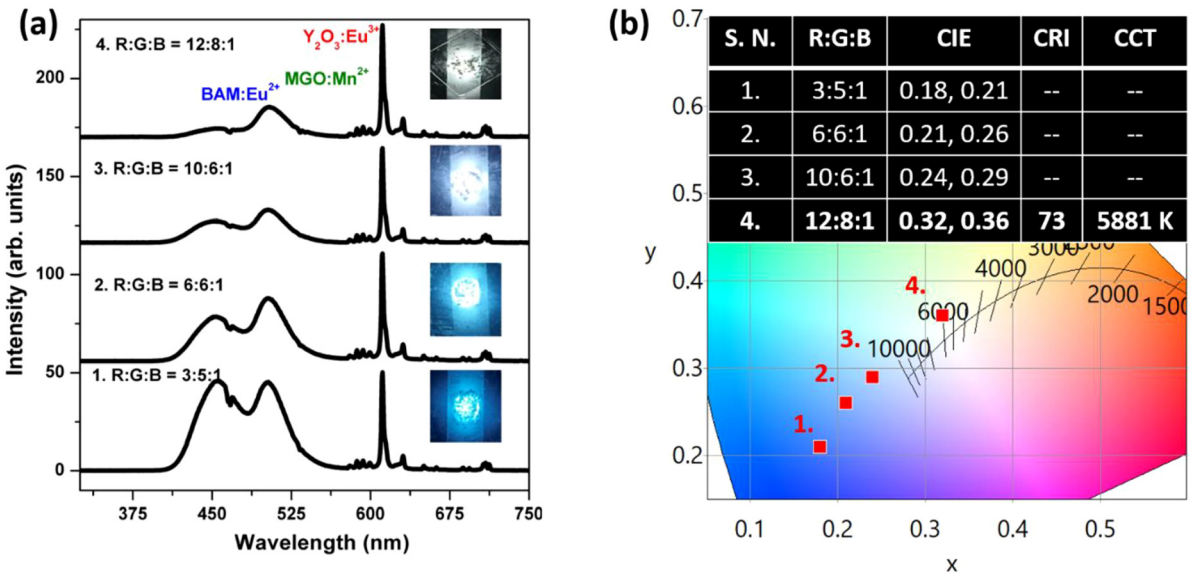

Fig. 10 (a) The EL spectrum of the mixture of Y_2O_3:Eu^{3+} red and BAM:Eu^{2+} blue and MGO-Mn(R) green phosphors. The mixture of RGB was taken in various ratios and combined with a 280 nm UV LED of current 3 mA. The direct images of the respective illuminated devices are included as the inset. (b) The CIE diagram of the corresponding EL spectra recorded at various RGB ratios.

Table 2 Comparison of the reported works on Mn^{2+} activated $MgGa_2O_4$ with this work

Work	Ref.
This work only reported excitation and emission spectra	66
This work has shown the stabilization of both Mn^{2+} and Mn^{4+} in $MgGa_2O_4$ and explored it for thermometry applications	67
This work is purely material synthesis work where authors have shown the effect of different kinds of fluxes on the PL of $MgGa_2O_4$:Mn^{2+} phosphors	68
This work reported the comparison between $MgGa_2O_4$:Mn^{2+} and $ZnGa_2O_4$:Mn^{2+} nanophosphors synthesized by the glycothermal method	69
This work is purely material synthesis work where authors have used the spray pyrolysis method, prevented surface residual non-radiative defect sites and produced highly luminescent and spherical phosphors	70
This is an upconversion paper where authors have reported the visible upconversion in Yb^{3+}, Mn^{2+} co-doped $MgGa_2O_4$ phosphors	71
We have reported bright green emission from $MgGa_2O_4$:Mn^{2+} with an IQE of 63% and EQE of 50% with a colour purity of 76.4%, which superseded that of the commercial green phosphor β-SiAlON:Eu^{2+}(59.12%) and carried out thermal stability measurements, thermoluminescence, afterglow under UV and X-ray and finally LED fabrication	This work

(Fig. 8c), reported elsewhere,[64,65] the activation energy for the present sample was estimated to be 0.31 eV. The CIE color coordinates were also measured for the emission spectra recorded at various temperatures ranging from 298 K to 438 K. The results presented in Fig. 8d clearly showed negligible variations in the measured coordinates at terminal temperatures, indicating the device potential of the present green phosphor.

3.6. Device performance

In order to check the credibility of the optimized green phosphor in white LED fabrication, a green pc-LED has been fabricated by mixing this green phosphor along with resin followed by coating the phosphor + resin mixture on a 280 nm UV LED source with an operating current of 3 mA. The resulting electroluminescence spectrum, shown in Fig. 9a, demonstrates a narrow band green emission at 504 nm with an FWHM of ~32 nm along with the LED spectral band situated at 280 nm. The resulting CIE coordinates can be seen from Fig. 9b, which are located in the green region, and the direct digital image of the illuminated pc-LED source is also depicted in the inset of the same figure. Such narrow band emission and appreciable thermal stability at elevated operating temperatures make the system suitable for white LED applications.

Finally, numerous white LEDs were made up using a mixture of commercial Y_2O_3:Eu^{3+}, an optimized green-emitting MGO-Mn(R) phosphor, and the commercial BAM:Eu^{2+} blue phosphor in various ratios. The different batches of powder mixtures were then mixed with resin and individually coated on identical 280 nm UV LED chips. Fig. 10a represents the EL spectra of the fabricated white LEDs with the various RGB mixing ratios along with the digital images of the respective illuminated devices in the insets. As seen in the CIE diagram depicted in Fig. 10b, by adjusting the RGB ratio at 12 : 8 : 1, the white light emission of the fabricated white LEDs shifted from cool white light to pure white light with a CCT of 5881 K and a CRI of 73, as observed from the CIE coordinates depicted in the inset of Fig. 10b.

Table 2 represents the reported works on Mn^{2+} doped $MgGa_2O_4$, which are compared with our work.

4. Conclusion

Here in this work, we have synthesized bright, pure and persistent deep green emitting MGO-Mn phosphors using the solid-state method. The synthesized phosphor was characterized by using XRD, FTIR, EDS and Raman spectroscopy. We could achieve an IQE of more than 63% and EQE of 50% in the sample annealed under a reduced atmosphere. The same sample was utilized in designing a pc-LED which showed deep green emission with a colour purity of 76.4%, which is superior to the commercial green phosphor. The optimum green phosphor can retain 61% at 423 K relative to the PL intensity observed at room temperature and the activation energy is estimated to be 0.31 eV, suggesting good thermal stability. In addition to this, the phosphor can be excited by using UV, visible and X-ray radiation, depicting efficient photo and radioluminescence. Interestingly both UV activation and X-ray activation show persistent luminescence properties driven by the presence of oxygen vacancy-related shallow traps. For evaluating the real-time device performance of the MGO-Mn phosphor, a prototype white-LED was fabricated by combining a 280 nm UV chip and a mixture of tri-color emitting phosphors, and by tuning the RGB phosphor composition, we could achieve both cool and pure white LEDs.

Data availability

The data are available from the corresponding author on reasonable request.

Conflicts of interest

There are no conflicts to declare.

Acknowledgements

The authors would like to acknowledge Dr Apurav Guleria, BARC Mumbai, for helping with Raman measurements and

Dr Jithendra Bahadur BARC Mumbai for FESEM and EDS measurements.

References

1 R. T. Parayil, S. K. Gupta, M. Abraham, S. Das, S. S. Pitale, K. Sudarshan and M. Mohapatra, Ultra-bright and thermally stable deep red emitting doped yttrium zirconate nanoparticles for tunable white LEDs and indoor plant growth, *Mater. Adv.*, 2023, **4**(22), 5594–5604.

2 T. P. R. Parayil, G. D. Patra, B. Modak, K. Sudarshan, M. Sonawane, S. Sen and S. K. Gupta, Uranium-Sensitized Luminescence Enhancement in Li2B4O7:U6+,Eu3+ and Potential Application towards Color-Tunable Phosphors and Actinide Sensor, *ACS Appl. Opt. Mater.*, 2023, **1**(1), 179–192.

3 T. Hasegawa, M. Iwaki, R. Tanaka, S.-W. Kim, S. Yin and K. Toda, Phase stabilization of red-emitting olivine-type NaMgPO4:Eu2+ phosphors via molten-phase quenching, *Inorg. Chem. Front.*, 2020, **7**(21), 4040–4051.

4 X. Zhang, J. Zhang, R. Wang and M. Gong, Photo-Physical Behaviors of Efficient Green Phosphor Ba2MgSi2O7:Eu2+ and Its Application in Light-Emitting Diodes, *J. Am. Ceram. Soc.*, 2010, **93**(5), 1368–1371.

5 J. H. Chung and J. H. Ryu, Photoluminescence and LED application of β-SiAlON:Eu2+ green phosphor, *Ceram. Int.*, 2012, **38**(6), 4601–4606.

6 E. H. Song, Y. Y. Zhou, Y. Wei, X. X. Han, Z. R. Tao, R. L. Qiu, Z. G. Xia and Q. Y. Zhang, A thermally stable narrow-band green-emitting phosphor MgAl2O4:Mn2+ for wide color gamut backlight display application, *J. Mater. Chem. C*, 2019, **7**(27), 8192–8198.

7 Q. Dong, J. Yang, J. Cui, F. Xu, F. Yang, J. Peng, F. Du, X. Ye and S. Yang, A narrow-band ultra-bright green phosphor for LED-based applications, *Dalton Trans.*, 2020, **49**(6), 1935–1946.

8 N. Latha, D. R. Lavanya, G. P. Darshan, B. R. Radha Krushna, H. B. Premkumar, H. C. Prameela and H. Nagabhushana, Green emanating BiOCl:Tb3+ phosphors for strategic development of dermatoglyphics and anti-counterfeiting applications, *Inorg. Chem. Commun.*, 2022, **138**, 109266.

9 Y. Hua and J. S. Yu, Strong Green Emission of Erbium(III)-Activated La2MgTiO6 Phosphors for Solid-State Lighting and Optical Temperature Sensors, *ACS Sustainable Chem. Eng.*, 2021, **9**(14), 5105–5115.

10 S. Wang, X. Liu, B. Qu, Z. Song, Z. Wang, S. Zhang, F. Wang, W.-T. Geng and Q. Liu, Green persistent luminescence and the electronic structure of β-Sialon:Eu2, *J. Mater. Chem. C*, 2019, **7**(40), 12544–12551.

11 B. Srivastava, S. Gupta, Y. Li and Y. Mao, Bright Persistent Green Emitting Water-Dispersible Zn2GeO4:Mn Nanorods, *Dalton Trans.*, 2020, **49**, 7328–7340.

12 J. S. Kim, H. J. Song, H.-S. Roh, D. K. Yim, J. H. Noh and K. S. Hong, Luminescent characteristics of green emitting Li2Ca2Si2O7:Eu2+ phosphor, *Mater. Lett.*, 2012, **79**, 112–115.

13 G. Annadurai, M. Jayachandiran, S. M. M. Kennedy and V. Sivakumar, Synthesis and photoluminescence properties of $Ba_2CaZn_2Si_6O_{17}$:Tb^{3+} green phosphor, *Mater. Sci. Eng., B*, 2016, **208**, 47–52.

14 Y. Xia, Y.-G. Liu, Z. Huang, M. Fang, M. S. Molokeev and L. Mei, Ca6La4(SiO4)2(PO4)4O2:Eu2+: a novel apatite green-emitting phosphor for near-ultraviolet excited w-LEDs, *J. Mater. Chem. C*, 2016, **4**(21), 4675–4683.

15 Y. Zhuo, S. Hariyani, J. Zhong and J. Brgoch, Creating a Green-Emitting Phosphor through Selective Rare-Earth Site Preference in NaBaB9O15:Eu^{2+}, *Chem. Mater.*, 2021, **33**(9), 3304–3311.

16 M. Zhao, H. Liao, L. Ning, Q. Zhang, Q. Liu and Z. Xia, Next-Generation Narrow-Band Green-Emitting RbLi(Li3SiO4)2:Eu2+ Phosphor for Backlight Display Application, *Adv. Mater.*, 2018, **30**(38), 1802489.

17 D. Jia, J. Zhu, B. Wu and S. E, Luminescence and energy transfer in CaAl4O7:Tb3+, Ce3+, *J. Lumin.*, 2001, **93**(2), 107–114.

18 S. Wang, B. Devakumar, Q. Sun, J. Liang, L. Sun and X. Huang, Highly efficient near-UV-excitable Ca2YHf2Al3O12:Ce3+,Tb3+ green-emitting garnet phosphors with potential application in high color rendering warm-white LEDs, *J. Mater. Chem. C*, 2020, **8**(13), 4408–4420.

19 J. Xue, H. M. Noh, S. H. Park, B. R. Lee, J. H. Kim and J. H. Jeong, NUV light induced visible emission in Er3+-activated NaSrLa(MoO4)O3 phosphors for green LEDs and thermometer, *J. Am. Ceram. Soc.*, 2020, **103**(2), 1174–1186.

20 Y. Li, Q. Yang, Z. Wang, G. Wang, B. Zhang, Q. Zhang and D. Yang, Rapid fabrication of SnO2 nanoparticle photocatalyst: computational understanding and photocatalytic degradation of organic dye, *Inorg. Chem. Front.*, 2018, **5**(12), 3005–3014.

21 C. Li, Z. Zang, W. Chen, Z. Hu, X. Tang, W. Hu, K. Sun, X. Liu and W. Chen, Highly pure green light emission of perovskite $CsPbBr_3$ quantum dots and their application for green light-emitting diodes, *Opt. Express*, 2016, **24**(13), 15071–15078.

22 X. Shen, C. Sun, X. Bai, X. Zhang, Y. Wang, Y. Wang, H. Song and W. W. Yu, Efficient and Stable CsPb(Br/I)3@Anthracene Composites for White Light-Emitting Devices, *ACS Appl. Mater. Interfaces*, 2018, **10**(19), 16768–16775.

23 P. Strobel, S. Schmiechen, M. Siegert, A. Tücks, P. J. Schmidt and W. Schnick, Narrow-Band Green Emitting Nitridolithoalumosilicate Ba[Li2(Al2Si2)N6]:Eu2+ with Framework Topology whj for LED/LCD-Backlighting Applications, *Chem. Mater.*, 2015, **27**(17), 6109–6115.

24 Y. Ito, T. Hori, T. Kusunoki, H. Nomura and H. Kondo, A phosphor sheet and a backlight system providing wider color gamut for LCDs, *J. Soc. Inf. Disp.*, 2014, **22**(8), 419–428.

25 T. Takeda, N. Hirosaki, S. Funahshi and R.-J. Xie, Narrow-Band Green-Emitting Phosphor Ba2LiSi7AlN12:Eu2+ with High Thermal Stability Discovered by a Single Particle Diagnosis Approach, *Chem. Mater.*, 2015, **27**(17), 5892–5898.

26 Y. Zhu, Y. Liang, S. Liu, H. Li and J. Chen, Narrow-Band Green-Emitting Sr2MgAl22O36:Mn2+ Phosphors with Superior Thermal Stability and Wide Color Gamut for Backlighting Display Applications, *Adv. Opt. Mater.*, 2019, **7**(6), 1801419.

27 H. Li, Y. Liang, S. Liu, W. Zhang, Y. Bi, Y. Gong and W. Lei, Highly Efficient Green-Emitting Phosphor BaZnAl10O17: Mn2+ with Ultra-Narrow Band and Extremely Low Thermal Quenching for Wide Color Gamut LCD Backlights, *Adv. Opt. Mater.*, 2021, **9**(24), 2100799.

28 C. Bertail, S. Maron, V. Buissette, T. Le Mercier, T. Gacoin and J.-P. Boilot, Structural and Photoluminescent Properties of Zn_2SiO_4:Mn^{2+} Nanoparticles Prepared by a Protected Annealing Process, *Chem. Mater.*, 2011, **23**(11), 2961–2967.

29 Y. Hu, Y. Yang, X. Zhang, X. Wang, X. Li, Y. Li, T. Li and H. Zhang, X-ray-Excited Super-Long Green Persistent Luminescence from Tb3+ Monodoped β-NaYF4, *J. Phys. Chem. C*, 2020, **124**(45), 24940–24948.

30 S. Vaidyanathan, Recent progress on lanthanide-based long persistent phosphors: an overview, *J. Mater. Chem. C*, 2023, **11**(26), 8649–8687.

31 A. Balhara, S. K. Gupta, M. Abraham, B. Modak, S. Das, C. Nayak, H. V. Annadata and M. Tyagi, Trap esngineering through chemical doping for ultralong X-ray persistent luminescence and anti-thermal quenching in Zn_2GeO_4, *J. Mater. Chem. C*, 2024, **12**(5), 1728–1745.

32 S. K. Gupta, B. Modak, M. Abraham, S. Das, R. Gupta, K. G. Girija, M. Mohapatra and K. Sudarshan, Defect induced tunable light emitting diodes of compositionally modulated zinc gallium germanium oxides, *Chem. Eng. J.*, 2023, **474**, 145595.

33 T. Hu, H. Lin, J. Xu, B. Wang, J. Wang and Y. Wang, Color-tunable persistent luminescence in oxyfluoride glass and glass ceramic containing Mn2+:α-Zn2SiO4 nanocrystals, *J. Mater. Chem. C*, 2017, **5**(6), 1479–1487.

34 M. Ma, L. Li, C. Cai, Y. Han and Y. Yang, X-ray excited (Mg, Ca)F2:Mn2+ for persistent luminescence modulation, *J. Lumin.*, 2022, **252**, 119376.

35 J. Xue, F. Li, F. Liu, H. M. Noh, B. R. Lee, B. C. Choi, S. H. Park, J. H. Jeong and P. Du, Designing ultra-highly efficient Mn2+-activated Zn2GeO4 green-emitting persistent phosphors toward versatile applications, *Mater. Today Chem.*, 2022, **23**, 100693.

36 R. T. Parayil, S. K. Gupta and M. Mohapatra, A review on defect engineered NIR persistent luminescence through transition metal ion (Cr, Mn, Fe and Ni) doping: Wider perspective covering synthesis, characterization, fundamentals and applications, *Coord. Chem. Rev.*, 2025, **522**, 216200.

37 B. Jiang, F. Chi, X. Wei, Y. Chen and M. Yin, A self-activated MgGa2O4 for persistent luminescence phosphor, *J. Appl. Phys.*, 2018, **124**(6), 063101.

38 A. Mondal and J. Manam, Structural and Luminescent Properties of Si4+ Co-Doped MgGa2O4:Cr3+ Near Infra-Red Long Lasting Phosphor, *ECS J. Solid State Sci. Technol.*, 2017, **6**(7), R88.

39 A. Mondal, S. Das and J. Manam, Hydrothermal synthesis, structural and luminescent properties of a Cr^{3+} doped $MgGa_2O_4$ near-infrared long lasting nanophospor, *RSC Adv.*, 2016, **6**(86), 82484–82495.

40 K. Girija, S. Thirumalairajan, V. R. Mastelaro and D. Mangalaraj, Photocatalytic degradation of organic pollutants by shape selective synthesis of β-Ga2O3 microspheres constituted by nanospheres for environmental remediation, *J. Mater. Chem. A*, 2015, **3**(6), 2617–2627.

41 T. Naka, T. Nakane, S. Ishii, M. Nakayama, A. Ohmura, F. Ishikawa, A. de Visser, H. Abe and T. Uchikoshi, Cluster glass transition and relaxation in the random spinel $CoGa_2O_4$, *Phys. Rev. B: Condens. Matter Mater. Phys.*, 2021, **103**(22), 224408.

42 P. Liu, Y. Zhang, B. Li, L. Han and Y. Xu, Trap depth engineering in MgGa2O4: Bi3+ for muticolor dynamic anti-counterfeiting, encryption and optical temperature sensing applications, *Chem. Eng. J.*, 2022, **437**, 135389.

43 N. Li, J. Liu, X. Duan, F. Yu and H. Jiang, Synthesis and microstructure of Co/Ni: MgGa2O4 nanoparticles, *J. Nanopart. Res.*, 2017, **19**(8), 285.

44 R. T. Parayil, S. K. Gupta, M. Pal, A. Dutta, D. Tyagi, K. Sudarshan and M. Mohapatra, $ZnGa_{2-x}Al_xO_4$ ($x = 0 \leq 2$) spinel for persistent light emission and HER/OER bi-functional catalysis, *RSC Adv.*, 2023, **13**(44), 31101–31111.

45 C. Yu, L. Zhang, J. Shi, J. Zhao, J. Gao and D. Yan, A Simple Template-Free Strategy to Synthesize Nanoporous Manganese and Nickel Oxides with Narrow Pore Size Distribution, and Their Electrochemical Properties, *Adv. Funct. Mater.*, 2008, **18**(10), 1544–1554.

46 R. T. Parayil, S. K. Gupta, K. Garg, S. Jangra, S. Samanta, K. Sudarshan, M. Mohapatra and T. C. Nagaiah, Enhanced electrocatalytic performance of bismuth-doped zinc stannate towards OER and HER through oxygen vacancies: p-block metal ion doping empowering d-block, *Sustainable Energy Fuels*, 2024, **8**(14), 3136–3144.

47 R. T. Parayil, S. K. Gupta, K. Garg, S. Mehta, K. Sudarshan, M. Mohapatra and T. C. Nagaiah, Improved catalytic activity on transitioning from inverse to normal spinel in Zn2−xGa2xSn1−xO4: a robust bifunctional OER and HER electrocatalyst, *Sustainable Energy Fuels*, 2024, **8**(10), 2144–2152.

48 N. Singh, V. Singh, G. Sivaramaiah, J. L. Rao, P. K. Singh, M. S. Pathak, S. J. Dhoble and M. Mohapatra, EPR and optical properties of Eu2+ and Mn2+ co-doped MgSrAl10O17 blue–green light emitting powder phosphors, *J. Lumin.*, 2016, **178**, 479–486.

49 Q. Zhou, L. Dolgov, A. M. Srivastava, L. Zhou, Z. Wang, J. Shi, M. D. Dramićanin, M. G. Brik and M. Wu, Mn2+ and

Mn4+ red phosphors: synthesis, luminescence and applications in WLEDs. A review, *J. Mater. Chem. C*, 2018, **6**(11), 2652–2671.

50 Y. Li, S. Qi, P. Li and Z. Wang, Research progress of Mn doped phosphors, *RSC Adv.*, 2017, **7**(61), 38318–38334.

51 Y. Feng, R. Liu, L. Zhang, Z. Li, Y. Su and Y. Lv, Raspberry-Like Mesoporous $Zn_{1.07}Ga_{2.34}Si_{0.98}O_{6.56}$:$Cr_{0.01}$ Nanocarriers for Enhanced Near-Infrared Afterglow Imaging and Combined Cancer Chemotherapy, *ACS Appl. Mater. Interfaces*, 2019, **11**(48), 44978–44988.

52 M. Liao, Q. Wang, Q. Lin, M. Xiong, X. Zhang, H. Dong, Z. Lin, M. Wen, D. Zhu, Z. Mu and F. Wu, Na Replaces Rb towards High-Performance Narrow-Band Green Phosphors for Backlight Display Applications, *Adv. Opt. Mater.*, 2021, **9**(17), 2100465.

53 Y. Pan, Y. Tang, X. Yin, M. Qiang, X. Yao and D. Zhang, ZnAl2O4:Mn2+ transparent phosphor ceramic with narrow-band green emission by spark plasma sintering, *J. Lumin.*, 2024, **265**, 120198.

54 C. Wang, X. Wang, Y. Zhou, S. Zhang, C. Li, D. Hu, L. Xu and H. Jiao, An Ultra-Broadband Near-Infrared Cr3+-Activated Gallogermanate Mg3Ga2GeO8 Phosphor as Light Sources for Food Analysis, *ACS Appl. Electron. Mater.*, 2019, **1**(6), 1046–1053.

55 Y. Yan, H. Dai, J. Li, C. Wang, W. Zhang and G. Zhu, Narrow-band green-emitting Cs3ZnCl5: Mn2+ phosphors with abnormal thermal quenching, *J. Lumin.*, 2023, **258**, 119821.

56 B. Wang, Y. Kong, Z. Chen, X. Li, S. Wang and Q. Zeng, Thermal stability and photoluminescence of Mn2+ activated green-emitting feldspar phosphor SrAl2Si2O8: Mn2+ for wide gamut w-LED backlight, *Opt. Mater.*, 2020, **99**, 109535.

57 G. Lu, Y. Wang, K. Ma, X. Chen, W. Geng, T. Liu, S. Xu, J. Zhang and B. Chen, A high-efficiency near-ultraviolet excited Mn2+ doped narrow-band emission phosphor via a strong charge transfer for wide color gamut WLED, *Ceram. Int.*, 2024, **50**(9, Part B), 16190–16200.

58 H. Chen and Y. Wang, Photoluminescence and cathodoluminescence properties of novel rare-earth free narrow-band bright green-emitting ZnB2O4:Mn2+ phosphor for LEDs and FEDs, *Chem. Eng. J.*, 2019, **361**, 314–321.

59 R. Cao, D. Peng, H. Xu, S. Jiang, Z. Luo, H. Ao and P. Liu, Synthesis and luminescence properties of $NaAl_{11}O_{17}$:Mn^{2+} green phosphor for white LEDs, *J. Lumin.*, 2016, **178**, 388–391.

60 Y. Fang, Y. Li, C. Wang, W. Yin, T. Shi, G. Zhang, G. Zhao, X. Zhou, J. Yang, D. Wu, L. Dong and J. Hou, Intense green light emission in Sr2ZnGe2O7:Mn2+ phosphors by the design of high symmetry melilite structure, *Luminescence*, 2024, **39**(1), e4555.

61 Z. Wu, C. Li, F. Zhang, S. Huang, F. Wang, X. Wang and H. Jiao, High-performance ultra-narrow-band green-emitting phosphor LaMgAl11O19:Mn2+ for wide color-gamut WLED backlight displays, *J. Mater. Chem. C*, 2022, **10**(19), 7443–7448.

62 X. Wu, Y. Liang, Y. Xue, H. Li, Y. Dou, W. Zhang, Q. Wang and C. Han, Synthesis and luminescence properties of a novel narrow band green-emitting Na2MgAl10O17:Mn2+ phosphor for backlight display, *J. Alloys Compd.*, 2024, **990**, 174397.

63 K. A. Denault, J. Brgoch, M. W. Gaultois, A. Mikhailovsky, R. Petry, H. Winkler, S. P. DenBaars and R. Seshadri, Consequences of Optimal Bond Valence on Structural Rigidity and Improved Luminescence Properties in SrxBa2−xSiO4:Eu2+ Orthosilicate Phosphors, *Chem. Mater.*, 2014, **26**(7), 2275–2282.

64 M. Abraham, A. K. Kunti, K. K. Thejas, N. Amador-Mendez, N. Gogneau, K. G. Nishanth, M. Tchernycheva and S. Das, The elevated colour rendering of white-LEDs by microwave-synthesized red-emitting (Li, Mg)$_3$$RbGe_8O_{18}$:$Mn^{4+}$ nano-phosphors, *Dalton Trans.*, 2021, **50**(8), 3044–3059.

65 M. Abraham, K. K. Thejas, A. K. Kunti, N. Amador-Mendez, R. Hernandez, J. Duras, K. G. Nishanth, S. K. Sahoo, M. Tchernycheva and S. Das, Strategically Developed Strong Red-Emitting Oxyfluoride Nanophosphors for Next-Generation Lighting Applications, *Adv. Opt. Mater.*, 2024, 2401356.

66 G. K. B. Costa, S. S. Pedro, I. C. S. Carvalho and L. P. Sosman, Preparation, structure analysis and photoluminescence properties of $MgGa_2O_4$:Mn^{2+}, *Opt. Mater.*, 2009, **31**(11), 1620–1627.

67 B. Zhu, L. Wang, Q. Shi, H. Guo, J. Qiao, C. E. Cui and P. Huang, $MgGa_2O_4$:Mn^{2+}, Mn^{4+}: A dual-emitting phosphors with unique optical temperature sensing, *J. Alloys Compd.*, 2023, **948**, 169717.

68 W. Ahn, M. Im and Y. J. Kim, Effects of flux on the luminescence of $MgGa_2O_4$:Mn^{2+} phosphors, *Mater. Res. Bull.*, 2017, **96**, 254–257.

69 M. Takesada, M. Osada and T. Isobe, Glycothermal Synthesis and Photoluminescence of $MgGa_2O_4$:Mn^{2+} Nanophosphors: Comparison to $ZnGa_2O_4$:Mn^{2+} Nanophosphors, *J. Electrochem. Soc.*, 2009, **156**(5), J97.

70 S. Choi, K. Kim, Y.-M. Moon, B.-Y. Park and H.-K. Jung, Rapid synthesis of spherical-shaped green-emitting $MgGa_2O_4$:Mn^{2+} phosphor via spray pyrolysis, *Mater. Res. Bull.*, 2010, **45**(8), 979–981.

71 E. H. Song, J. L. Wang, D. C. Yu, S. Ye and Q. Y. Zhang, Anomalous tunable visible to near infrared emission in the Mn^{2+}-doped spinel $MgGa_2O_4$ and room-temperature upconversion in the Mn^{2+} and Yb^{3+}-codoped spinel, *J. Mater. Chem. C*, 2014, **2**(41), 8811–8816.